Role of N defects in paramagnetic CrN at finite temperatures from first principles

E. Mozafari,[1,*] B. Alling,[1] P. Steneteg,[1] and Igor A. Abrikosov[1,2,3]
[1]*Department of Physics, Chemistry and Biology, Linköping University, SE-58183 Linköping, Sweden*
[2]*Materials Modeling and Development Laboratory, NUST "MISIS", 119049 Moscow, Russia*
[3]*LOCOMAS Laboratory, Tomsk State University, 634050 Tomsk, Russia*
(Received 21 October 2014; published 2 March 2015)

Simulations of defects in paramagnetic materials at high temperature constitute a formidable challenge to solid-state theory due to the interaction of magnetic disorder, vibrations, and structural relaxations. CrN is a material where these effects are particularly large due to a strong magnetolattice coupling and a tendency for deviations from the nominal 1:1 stoichiometry. In this work, we present a first-principles study of nitrogen vacancies and nitrogen interstitials in CrN at elevated temperature. We report on formation energetics, the geometry of interstitial nitrogen dimers, and the impact on the electronic structure caused by the defects. We find a vacancy formation energy of 2.28 eV with a small effect of temperature, i.e., a formation energy for N interstitial in the form of a ⟨111⟩-oriented split bond of 3.77 eV with an increase to 3.97 at 1000 K. Vacancies are found to add three electrons, while split-bond interstitial adds one electron to the conduction band. The band gap of defect-free CrN is smeared out due to vibrations, although it is difficult to draw a conclusion about the exact temperature at which the band gap closes from our calculations. However, it is clear that at 900 K there is a nonzero density of electronic states at the Fermi level. At 300 K, our results indicate a border case where the band gap is about to close.

DOI: 10.1103/PhysRevB.91.094101 PACS number(s): 75.10.−b, 75.20.En, 75.20.Hr, 71.15.Pd

I. INTRODUCTION

Transition-metal nitrides (TMNs) belong to the hard refractory materials which typically crystallize in the rocksalt structure. They are widely used as hard protective coatings on cutting tools and for coatings in metal-forming or plastic-moulding applications [1,2]. Among these, chromium nitride has in addition to its practical applications been of interest due to its fascinating magnetic, optical, and electronic properties. It is well known that CrN is paramagnetic with a $B1$ structure at room temperature, while at Néel temperature (T_N), in the range between 270–286 K, it undergoes a phase transition to antiferromagnetic (AFM) with orthorhombic structure [3–5]. Theoretically the magnetic stress is thought to be the driving force for the lattice distortions [6,7]. Thus the magnetic transition at temperatures around 280 K is associated with the structural transition [3]. On the other hand, no sign of magnetic ordering has been observed in epitaxially stabilized cubic CrN thin films [8–10]. The importance of the electron correlations in CrN has recently been shown experimentally [11]. Most of the theoretical calculations have considered only ordered magnetic structures [6,7,12] despite the fact that most experimental measurements are carried out above the Neél temperature.

In 2009, Rivadulla *et al.* reported that the bulk modulus of CrN collapses at high pressures [4], but their theoretical modeling neglected the interplay between the magnetism and structure on the local level as well as globally in the paramagnetic regime. Theoretical modeling taking disordered magnetism into account did not find any dramatic changes in compressibility [13]. Later experiments confirmed the absence of elastic softening upon the phase transition [5]. In other words, above the critical Curie or Neél temperature, there are examples of fully itinerant Stoner magnets, but most magnetic systems, and CrN in particular, retain their magnetic moments even though the long-range order between them is lost. Thus, when performing first-principles calculations, a disordered magnetic configuration must be considered to simulate and fully understand the physical properties of paramagnetic CrN at elevated temperatures [13]. It should be noted that magnetic materials above the magnetic transition temperature are not only spatially disordered, but also dynamically disordered. Thus, at higher temperatures, the magnetic moments are changing randomly over time. Alling *et al.* [14] performed a detailed study on the effect of the magnetic disorder on the thermodynamics of paramagnetic CrN using the disordered local-moment method (DLM) implemented within two supercell frameworks, i.e., the magnetic sampling method (MSM) and the special quasirandom structure method (SQS). In their work, they obtained an orthorhombic to cubic phase-transition temperature as a function of pressure qualitatively in line with, but quantitatively higher than, the experimental measurements. It was suggested that the magnetic short-range order coupled to the vibrational degrees of freedom should also be of importance in order to determine the transition temperature in CrN. The importance of the vibrations was the main motivation behind Steneteg's work merging the disordered local-moment model with *ab initio* molecular dynamics (DLM-MD) [15]. Recently, the effect of vibrations on the phase transition was investigated [16] by DLM-MD combined with the temperature-dependent effective potential (TDEP) [17] method and spin state averaging phonon calculations [18]. The effects of vibrations on the magnetic exchange interactions of CrN were studied with the magnetic direct cluster averaging method by Lindmaa *et al.* [19]. Furthermore, $Ti_{1-x}Cr_xN$ [20] and $Cr_{1-x}Al_xN$ [21] alloys have also been studied using these methods. Others have also investigated $Cr_{1-x}TM_xN$ alloys using the SQS approach [22],

*elhmo@ifm.liu.se

in which the Cr spin up and Cr spin down are randomly distributed in a disordered way in the supercell.

The electronic structure of CrN is another controversial issue. Depending on the experimental circumstances, some groups have observed CrN to exhibit semiconducting behavior in its AFM phase [23]. This conclusion has been supported by some band structure calculations [6,7] indicating that AFM CrN exhibits semiconducting behavior, whereas it behaves like a metal in its $B1$-rocksalt structure. This is in contradiction to measurements done by Herle *et al.* [24] and more recent experiments on rocksalt paramagnetic (PM) CrN showing an increase in the resistivity with decreasing temperature, indicating that it is a semiconductor [8,9,25], but the discussion is still open.

Thus far, almost all of the theoretical investigations of CrN-based materials have assumed a stoichiometric nitrogen sublattice. This is in contrast to the experiments where the stoichiometry of TMN films can depend strongly on the specific choice of the synthesis technique and, in the case of thin films, the choice of growth parameters. Therefore, the point defects are naturally present in the films. In particular, N vacancies (V_N) and also N interstitials (I_N) are believed to be important point defects existing in TMN films grown by physical vapor deposition techniques [26,27]. Several groups have experimentally studied how the electronic and mechanical properties of CrN change due to nitrogen stoichiometry [28–31].

The nature of the conduction in CrN is affected by vacancies and interstitials as they contribute with carriers and also induce defect states in the band structure. In general, the effect of defects and temperature-induced vibrations, especially in paramagnetic systems, remains unresolved. Due to the strong magnetolattice interactions in PM systems and their tendency to deviate from the nominal 1:1 stoichiometry, the effects of the interaction of magnetic disorder, vibrations, and structural relaxations are large. Thus more detailed and new methods are needed to study the behavior of the vacancy, interstitial, or substitutional atoms in paramagnetic materials.

In this article, the impact of N vacancies (V_N) and interstitials (I_N) on the electronic structures and the defect formation energies in the PM cubic CrN at finite temperature are studied.

II. CALCULATIONAL DETAILS

The formation energy of a single nitrogen defect is defined according to

$$E^F = E_{\text{def}} - E_{\text{TMN}} + \frac{x}{2}E_{N_2}, \tag{1}$$

in which E_{def} is the total energy of the system in the presence of the defect, E_{TMN} is the total energy of the host, defect-free CrN system, and E_{N_2} is the energy of the N_2 molecule in the vacuum. x can be either $+1$ for V_N or -1 for I_N defects.

In this work, all first-principles calculations are performed utilizing the projector augmented wave (PAW) method as implemented in the Vienna *Ab initio* Simulation Package (VASP) [32–34]. The Born-Oppenheimer molecular dynamics is used in our simulations. The paramagnetic state is approximated in our calculations through harnessing the disordered local-moment model, introduced by Hubbard [35–37] and Hasegawa [38,39] and applied within an electronic structure framework by Gyorffy [40]. Supercell implementations of DLM were investigated by Alling *et al.* [14] and the idea of combining the disordered local-moment model and molecular dynamics, DLM-MD, was introduced and implemented by Steneteg *et al.* [15], and has since been used to model mixing thermodynamics in $Cr_{1-x}Al_xN$ [21] and vibrational spectra of CrN [17]. In this work, we use both static supercell DLM and DLM-MD. The electronic exchange-correlation effects are modeled via a combination of local density approximation with a Hubbard Coulomb term (LDA+U) [41]. In this implementation of LDA+U, we have used the double-counting correction scheme suggested by Dudarev *et al.* [42]. The value of the $U^{\text{eff}} = U - J$ is taken to be 3 eV for Cr $3d$ orbitals, which is found to be the optimal value obtained theoretically from comparison of the structural and electronic properties of CrN with experimental measurements as reported in Ref. [14].

The energy cutoff for the expansion of the plane waves is 400 eV, unless stated otherwise. Using the Monkhorst-Pack scheme, the Brillouin zone is sampled on a $3 \times 3 \times 3$ grid containing 32 Cr and 32 N atoms when defects are not present. To obtain the density of states (DOS), a selection of configurations from MD steps is chosen and their electronic structure is recalculated with higher accuracy, that is, with an energy cutoff of 500 eV and a grid of $5 \times 5 \times 5$ k points.

The calculations are also done for a larger supercell of 216 atoms at $T = 0$ K for the defect-free system and when the defects are introduced. Due to the expensive calculations, DLM-MD calculations for the large supercell are done only at two different temperatures to evaluate the vacancy formation energy.

The simulations are carried out considering a canonical ensemble (NVT). In order to control the temperature of the simulation, the standard Nosé thermostat [43] is used as implemented in VASP with the default Nosé mass set by the package.

The lattice constant of CrN is set to its calculated equilibrium zero-temperature value, 4.129 Å. It is worth mentioning that we also ran several calculations using the experimental lattice constants ranging from 4.15 to 4.18 Å at specific temperatures, i.e., we consider the effect of thermal expansion according to experiments.

In order to model the paramagnetic state in the static calculations, we have used the magnetic sampling method (MSM) [14]. Within this approximation, the directions of the magnetic moments (up and down) of the Cr atoms for the 64-atom supercell are randomly distributed. A set of such samples with different magnetic configurations surrounding the defect and the constraint of a net total zero magnetization in the supercell are then created. Each of these configurations are fully relaxed and their energies are calculated. The defect-free CrN system with different magnetic configurations is also sampled. All of the configurations are relaxed and the average energy is calculated which gives us the term E_{TMN} in Eq. (1). The reported energy for static calculations in this paper is the average energy of these calculations, which is chosen as

the energy of the fictitious paramagnetic disordered state at 0 K [44]. It should be noted that the magnetically induced lattice relaxations are artificial consequences of the static magnetic order. However, the energies of these relaxations are likely to cancel if the same order is used in the defect-containing and pure CrN cell of Eq. (1). At least this was the case for the $Cr_{1-x}Al_xN$ in Ref. [21].

The DLM-MD model is introduced to simulate the paramagnetic materials at finite temperatures. In this method, the local magnetic moments are considered to be disordered and the magnetic state of the system is changed in a stochastic way with a given period during the MD simulation. In other words, the simulation starts with a random magnetic configuration and an MD simulation is run for some time during which the magnetic state is fixed. The magnetic configuration of the system is then substituted with another random set of moments, the MD is then continued, and the process goes on until the given simulation time is finished. The time span between which the magnetic configuration is being kept fixed is called the "spin-flip time," Δt_{sf}. During our simulations, Δt_{sf} is chosen to be 5 fs, which according to Ref. [15] should practically correspond to adiabatic approximation with fast moments. The potential energy of the atomic system, basically the total energy minus the kinetic energy of the ions, is extracted from the DLM-MD calculations. The energy of the system E_{TMN} or, in the case of defects, E_{def} is then obtained by averaging over the energies of the DLM-MD time steps. Using Eq. (1), one can then calculate the formation energies of a specific temperature at which the simulation is carried out. We have to mention also that the temperature dependence of the N_2 molecule, E_{N_2}, in Eq. (1) is not included. We have used the 0 K value of E_{N_2} for obtaining the formation energies, as our focus is to investigate if the lattice vibrations influence defect thermodynamics. The effect of gas phase thermodynamics is outside of the topic of this work.

III. RESULTS

In the following, we will describe in detail the results obtained for CrN including nitrogen vacancy and interstitial nitrogen. We first discuss the nitrogen vacancy case and then we consider the nitrogen interstitials.

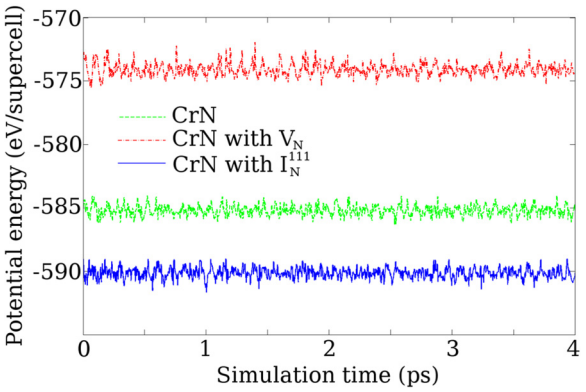

FIG. 1. (Color online) Potential energy of paramagnetic CrN as a function of simulation time calculated at $T = 300$ K using the DLM-MD method. The figure also includes the potential energy of cubic CrN in the presence of N vacancy and N interstitial (I_N^{111}) calculated at the same temperature.

A. N vacancy

1. Static supercell DLM

The first type of N defects corresponds to nitrogen vacancies. By relaxing the supercell containing only a single vacancy, we found that the N vacancy will produce an outward relaxation in the surrounding CrN matrix, in agreement with what is obtained by Jhi *et al.* [45] and Tsetseris *et al.* [46,47] for TiN, ZrN, and HfN.

In order to calculate the formation energy via the magnetic sampling method in combination with the special quasirandom structure method (MSM-SQS) [44], the vacancy is moved around in a $2 \times 2 \times 2$ conventional unit cell with magnetic state set according to the SQS-DLM method, placing it in different magnetic local environments. The average energy of the MSM-SQS calculations is considered as the E_{def} term in Eq. (1). The calculated vacancy formation energy is 2.28 eV/supercell as reported in Table. I.

2. DLM-MD

The DLM-MD simulations are performed at different temperatures for a k-point grid of $3 \times 3 \times 3$. Figure 1 shows the extracted potential energy from DLM-MD calculations at

TABLE I. Relative stability of nitrogen point defects in paramagnetic CrN obtained from static DLM and DLM-MD calculations at six different temperatures.

Defect	Geometry	E^F [a](eV/defect) Static DLM	E^F(eV/defect) DLM-MD					
			300 K	600 K	700 K	900 K	1000 K	1200 K
V_N		2.28	2.37	2.40	2.38	2.32	2.37	2.30
I_N^{tet}	Tetrahedral	Metastable[b]	[c]					
I_N^{110}	Split bond ⟨110⟩	3.84	[c]					
I_N^{111}	Split bond ⟨111⟩	3.77	3.80	3.84	3.87	3.87	3.97	3.88

[a]The energies are obtained from MSM.

[b]During our MSM calculations, we noticed that an interstitial in the tetrahedral configuration would either remain in the tetrahedral position or go into the split-bond I_N^{111} configuration (see the text).

[c]DLM-MD calculations at various temperatures show that the tetrahedral and the split-bond ⟨110⟩ configurations are unstable. Instead, the N-N pair positions itself along the ⟨111⟩ direction.

a specific temperature of $T = 300$ K and, as can be seen, the potential energy is well conserved. The energy of the system, in the case of a defect $E_{\rm def}$, is obtained by averaging over all MD energies (red dot-dashed line for vacancy and blue solid line for interstitial). The energy $E_{\rm TMN}$ is also obtained from averaging over all the energies (green dashed line) of the CrN system in the absence of any defects. Obtaining the vacancy formation energies is then straightforward. The vacancy formation energies at six different temperatures are listed in Table I. It is apparent that there is not a large change in the vacancy formation energy as a function of temperature caused by vibrations. The given values show that E^F is varying between 2.30 to 2.40 eV/supercell at various temperatures but in a random way, indicating that it is a statistical noise and allowing us to estimate the error bar of 0.1 eV per defect using this method. And, of course, the free energy of the defect should depend on temperature via the entropy contribution. Also the vibrational entropy is not explicitly considered here [17].

The same calculations were performed for a larger defect-free supercell of 216 atoms consisting of 108 Cr atoms and 108 N atoms and also for a supercell with a vacancy of 107 N atoms. The vacancy formation energy at $T = 300$ K, in this case, is 2.35 eV/supercell.

Comparing the vacancy formation energies obtained from static supercell DLM calculations and also from DLM-MD as listed in Table I, we can conclude that the DLM-MD calculations in this case justify the static approximation. In particular, the good agreement between the static and DLM-MD calculations indicates that the artificial static relaxations present in the former method cancel each other, as they contribute almost equally to the the first and the second terms in the right-hand side of Eq. (1).

B. N interstitial

1. Static supercell DLM

The second class of point defects that we consider is N interstitials. In contrast to the vacancy defects, different N-interstitial positions are possible. Probably the most straightforward consideration is an I_N in a tetrahedral position, $I_N^{\rm tet}$, shown in Fig. 2(c). Other possible arrangements are the split-bond interstitials for which the excess N atom forms a N-N dimer, with one of the nitrogen atoms in the CrN matrix centered at the N lattice position. This dimer can be aligned in different directions. Figures 2(a) and 2(b) demonstrate two different arrangements with the N-N bond pointing in the ⟨110⟩ (I_N^{110}) and ⟨111⟩ (I_N^{111}) directions, respectively.

For harnessing the magnetic sampling method (MSM) in the case of interstitials, the excess nitrogen is kept in one position and the magnetic configuration of the Cr atoms surrounding it is changed. The energy $E_{\rm def}$ is calculated in the same way as discussed earlier in this paper and the formation energies are obtained using Eq. (1). In this case, the defect-free CrN is also calculated for each magnetic sample. The relative stability results for both split-bond and tetrahedral interstitials are summarized in Table. I. The formation energy of I_N^{110} is 3.84 eV/defect, which is 0.07 eV/defect higher in energy than the value obtained for I_N^{111}, i.e., 3.77 eV/defect. In the case of nitrogen interstitial in a tetrahedral position for a $2 \times 2 \times 2$ supercell consisting of 32 Cr atoms and 33 N atoms, we have done the calculations for 27 magnetic samples, out of which 14 configurations relaxed to a split bond I_N^{111}. The defect in the 13 other magnetic samples remained in the tetrahedral position. This can be interpreted to show that $I_N^{\rm tet}$ is, at best, a metastable site at $T = 0$ K. The N-N dimer bond length in the case of I_N^{111} is 1.27 Å, which is larger than the N_2 molecule bond length 1.1 Å, as calculated with the local-density approximation (LDA). In order to understand this situation, we also studied the formation energy and the bond length variation of the N interstitials as a function of temperature.

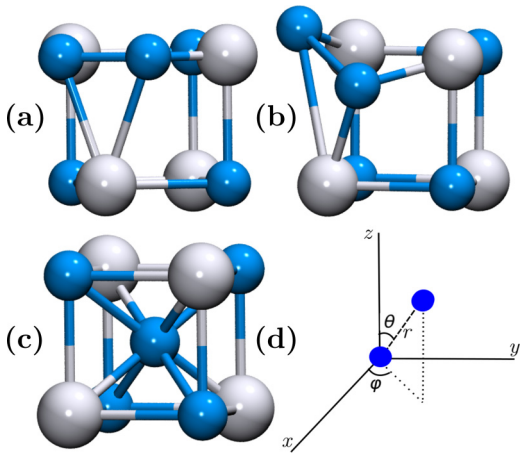

FIG. 2. (Color online) Possible N interstitial initial positions in the CrN unit cell. The blue circles show nitrogen and the gray circles are Cr atoms. The figure demonstrates N interstitial in the (a) I_N^{110} position, (b) I_N^{111} position, and (c) $I_N^{\rm tet}$ position. (d) The spherical coordinates related to the coordinates and lines depicted in Fig. 3.

2. DLM-MD

Figure 1 includes the potential energy of the system with a nitrogen interstitial in the split-bond I_N^{111} configuration at $T = 300$ K (the solid blue line). The potential energy is well conserved as for the nitrogen vacancy case. $E_{\rm def}$ is obtained by averaging over all DLM-MD energies. The formation energy is then calculated using Eq. (1).

The data obtained for the relative stability of nitrogen interstitials show that the only stable configuration at elevated temperatures is the split bond I_N^{111}. The I_N^{111} formation energies at different temperatures are summarized in Table I. Unlike the vacancy case, the formation energy of the nitrogen interstitial exhibits an increasing trend as the temperature increases. It starts from 3.80 eV/supercell at $T = 300$ K and rises to 3.97 eV/supercell at $T = 900$ K, except for the formation energy at $T = 1200$ K which drops to 3.88 eV/supercell. The same argument about the E_{N_2} term in Eq. (1), mentioned in the beginning of Sec. III, also applies here. In our calculations, E_{N_2} is considered to be temperature independent and its 0 K value is used in all cases.

In order to understand the relation between different interstitial positions, the nitrogen pair (the I_N and the N from the CrN lattice) dynamics is studied in Fig. 3. The figure depicts the I_N's bond vector (N-N bond) coordinates in a spherical coordinate system [see Fig. 2(d)] as a function of simulation

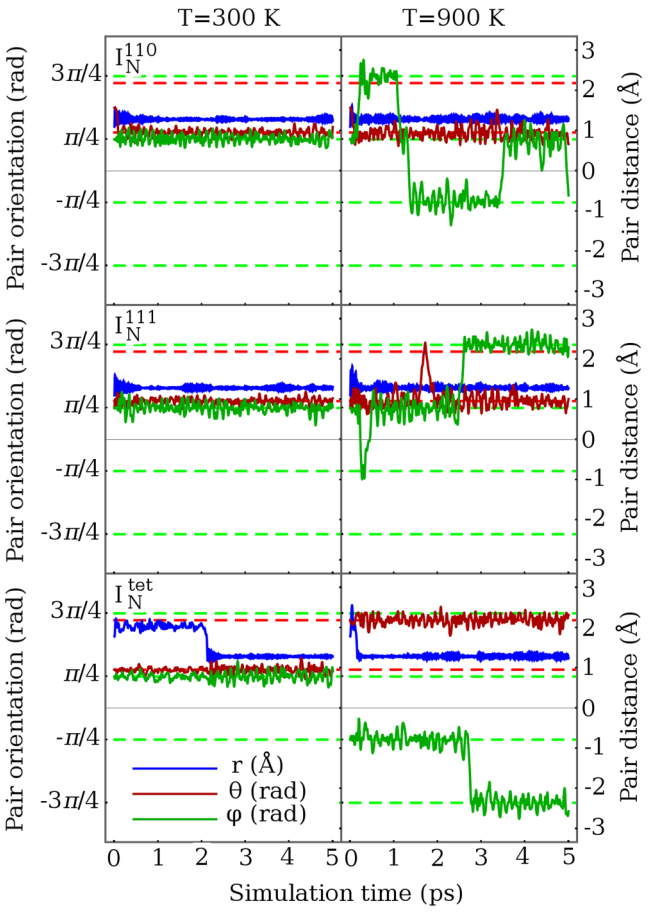

FIG. 3. (Color online) Nitrogen pair [N(I_N)-N(CrN)] dynamics in paramagnetic CrN as a function of simulation time at $T = 300$ K (left column) and $T = 900$ K (right column). Panels from top to bottom show split-bond $\langle 110\rangle$, split-bond $\langle 111\rangle$, and tetrahedral configurations, respectively. The spherical coordinate system used here is shown in Fig. 2. The blue color is the radial distance between the nitrogen pair in Å. The angles show the orientation of the N-N bond vector and the dashed lines represent all of the symmetry directions equivalent to the directions $\langle 111\rangle$, $\langle \bar{1}11\rangle$, $\langle 11\bar{1}\rangle$, $\langle 1\bar{1}1\rangle$, etc. The green color shows the azimuthal angle φ. The dashed green lines are different values of φ between 0 and 2π. The red solid and dashed lines show the polar angle θ which varies between 0 and π. In the case of I_N^{110}, the value of θ (red solid line) should be constant, $\pi/2$. However, as can be seen in the figure, θ changes to $\pi/3$ and vibrates around this value, indicating that the pair is in the $\langle 111\rangle$ direction.

time. From Fig. 3, it can be seen that the interstitial nitrogen in the tetrahedral position at $T = 300$ K transforms into the split bond after some time (~ 2 ps), seen in the N-N distance r. Figure 3 also demonstrates the same variables at $T = 900$ K. It is clear from the figure that both I_N^{110} and I_N^{tet} configurations transform into the I_N^{111} arrangement more or less immediately. The bond distance r is almost constant around 1.2 Å, while some variations can be distinguished in the polar angle φ in all three cases. The dashed lines show all the directions that are symmetry equivalent to the $\langle 111\rangle$ direction, namely, $\langle \bar{1}11\rangle$, $\langle 11\bar{1}\rangle$, $\langle 1\bar{1}1\rangle$, etc. At $T = 900$ K, starting from angle $\pi/4$, i.e., the green dotted line, the polar angle φ goes almost immediately to $3\pi/4$ in the case of I_N^{110} and oscillates around this value for a while; it then goes to $-\pi/4$, remains there for some time, and finally goes back to $\pi/4$. In the case of I_N^{111}, φ oscillates around $\pi/4$ at the beginning and goes to $3\pi/4$ after almost 2.5 ps. For the tetrahedral configuration, as mentioned, the interstitial transforms to the I_N^{111} position and the polar angle vibrates around $-\pi/4$ until 2.8 ps, after which it goes to $-3\pi/4$ and oscillates around this angle during the rest of the simulation. The azimuthal angle θ, on the other hand, is almost conserved and vibrates around the red dashed line, showing $\pi/3$ in I_N^{111} and around $2\pi/3$ in the tetrahedral case which is one of the equivalent directions to $\langle 111\rangle$, indicating that the tetrahedral N transforms to I_N^{111}. In the I_N^{110} case, θ should be $\pi/2$ and, as can be seen in Fig. 3, the red solid line starts from $\pi/2$ but, at both temperatures, it goes to $2\pi/3$ after a very short time. This indicates that the I_N^{110} configuration is unstable. It transforms to the I_N^{111} configuration and the N-N dimer continues vibrating along the $\langle 111\rangle$ direction. The changes in the angles are basically jumps between the directions equivalent by symmetry to the $\langle 111\rangle$ direction (for further information regarding the dynamics, see the Supplemental Material [48]).

To complete the picture, we also plotted the nitrogen pair position probability density to illustrate the spatial distribution of the N atoms during DLM-MD simulations. The red color shows the extra nitrogen added to the system and the blue color is the nitrogen from the CrN matrix pairing with the interstitial N. Where the density is higher indicates the position in which the nitrogen spends most of its time during the simulation. As can be seen in Fig. 4, the tetrahedral case at $T = 300$ K is in complete agreement with its counterpart in Fig. 3 in which the I_N^{tet} transforms to the I_N^{111} position after some time. It is also visible that the I_N^{110} moves to the I_N^{111} arrangement. The pair position probability density at $T = 900$ K is also shown in the right panel of Fig. 4.

The situation is similar for other temperatures, except for the fact that the higher the temperature is, the more vibration is seen in the plots and the probability densities look spatially more spread.

Studying the N-N pair bond length shows that the average bond distance of the dimer varies between 1.28 and 1.3 Å, depending on the temperature, which is in good agreement with the nitrogen pair distance reported in other TMNs [47]. The obtained value is somewhat larger than both the calculated (using LDA) and experimental value of the nitrogen molecule bond distance, 1.1 Å.

The movies obtained from DLM-MD calculations (see the Supplemental Material [48]) show that the N-N bond wants to have a particular orientation ($\langle 111\rangle$ direction). This is what is seen in Fig. 3. This actually indicates that the N-N dimer is not freely rotating in any direction. This implies that the nitrogen pair is, in fact, bonded to the CrN matrix. A free nitrogen molecule exhibits a triple bond but, according to the fact that the N-N bond is stretched and larger than 1.1 Å for N interstitial in CrN, we can argue that the nitrogen dimer is better described to have an internal double bond with two electrons, which can freely interact with the CrN lattice.

To critically evaluate this suggestion, the electronic structure study is needed. It is discussed in Sec. V.

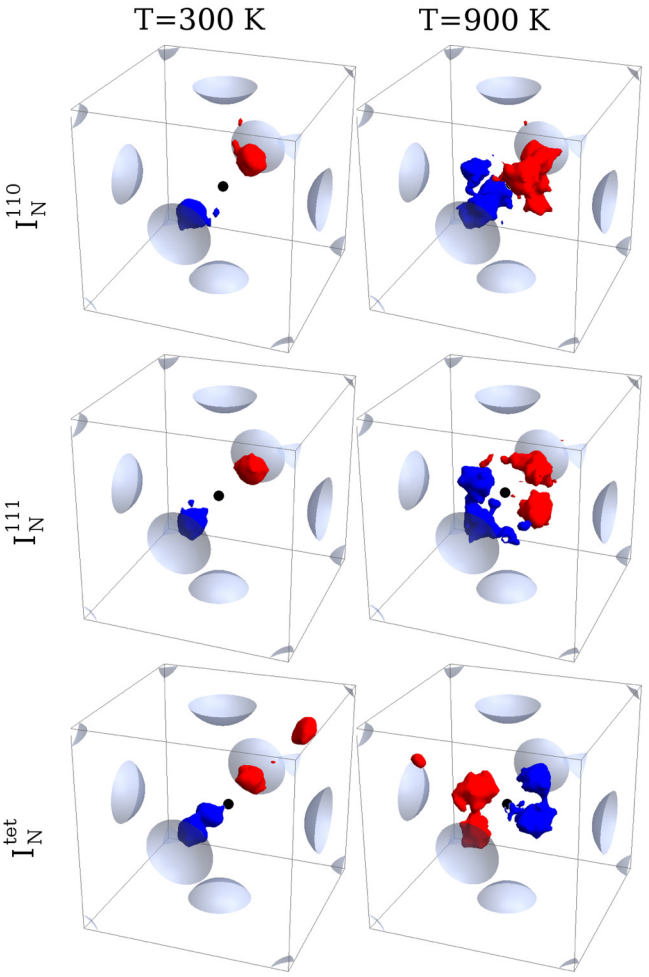

FIG. 4. (Color online) Nitrogen pair [N(I_N)-N(CrN)] probability density in paramagnetic CrN at $T = 300$ K (left column) and $T = 900$ K (right column). Panels from top to bottom show split-bond ⟨110⟩, split-bond ⟨111⟩, and tetrahedral geometries, respectively. The figure includes only the neighboring Cr atoms (gray). Red shows the interstitial nitrogen and blue is the nitrogen from the CrN matrix. The starting geometry is shown by a black circle. The blue and red colors are densities that show where the two nitrogens in the pair spend most of their time during the simulation. The densities follow the trend shown also in Fig. 3. For instance, the nitrogen in the tetrahedral configuration at $T = 300$ K transforms to the I_N^{111} position and remains there, as can be seen in the related panel in Fig. 3.

IV. MAGNETIC MOMENTS

CrN is a system with rather robust local magnetic moments on the Cr atoms. The net magnetization and the local moments for the case of defect-free CrN were calculated by means of the DLM-MD method in Ref. [15].

Figure 5 shows the evolution of the magnitude of the local magnetic moments of the cubic CrN in the presence of defects obtained from DLM-MD calculations at $T = 300$ K. As is mentioned in Sec. II, each of our DLM configurations will run for $\Delta t_{sf} = 5$ fs during which the magnetic configuration is kept fixed but the MD simulations will run, i.e., for each magnetic configuration, we will have five MD steps. From these five steps, we have only extracted the last step's magnetic

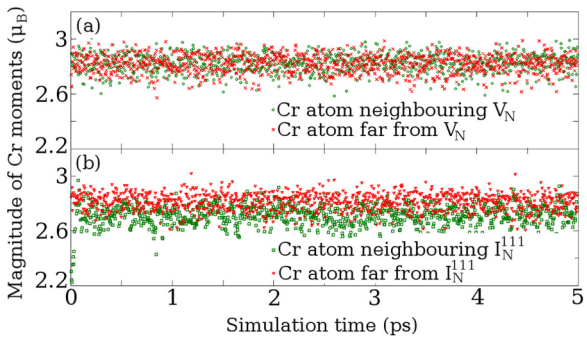

FIG. 5. (Color online) The evolution of the magnitude of the Cr magnetic moments, neighbor to the defect and further away from the defect as a function of simulation time for (a) nitrogen vacancy case and (b) nitrogen interstitial in the ⟨111⟩ case, carried out at $T = 300$ K.

moments. In other words, the magnetization is only given once for every magnetic flip. In both panels of Fig. 5, i.e., for the vacancy case [Fig. 5(a)] and for the I_N^{111} case [Fig. 5(b)], we have plotted the local moments at two Cr atoms. The Cr atoms are sitting in two different positions, one in the neighborhood of the defect and the other one further away from it. As can be seen, the magnetic moments are robust and it does not make a distinct difference where in the supercell the Cr atom is located, i.e., close to the defect or further away in the vacancy case. The magnitudes of the Cr local moments average to the same value of $M \sim 2.82\mu_B$, for spin up (positive) and spin down (negative). Similar behavior was reported in Refs. [14,15,20] for stoichiometric CrN. Local moments are stable during all of our simulations. Likewise, in the case of a Cr atom far from the interstitial, the same behavior is visible with the average $M \sim 2.81\mu_B$. However, for the Cr atom which is sitting in the neighborhood of the I_N^{111}, the magnitudes of the local magnetic moments average to a slightly smaller value of $M \sim 2.71\mu_B$. The small changes in the local magnetic moments amplitude, even in the direct vicinity of point defects, underline once again the robust character of the Cr moments in CrN.

V. ELECTRONIC STRUCTURE

We have studied the effect of the point defects on the electronic properties of cubic paramagnetic CrN. Figure 6 shows the density of states (DOS) of defect-free CrN obtained in static calculations using our approach along with the DOS of the system in the presence of point defects. The supercell consists of 32 Cr atoms and 32 N atoms in the defect-free case and 31 or 33 N atoms when vacancy or I_N^{111} interstitial is present. We have also calculated the density of states for a large supercell consisting of 216 atoms, i.e., 108 Cr and 108 N, and for the case of N vacancy with 107 N atoms (not shown here). Defects could add or remove electrons to the system which will be visible as a shift to the Fermi level with respect to the bands in a defect-free supercell. They will affect the conductivity of the material. Such effects are apparent in Fig. 6, where there is a small gap at the Fermi level in the absence of nitrogen defects, in agreement with the previous studies [14]. The presence of a defect results in the closing of this very narrow gap. As can be seen in Fig. 6 (blue dashed

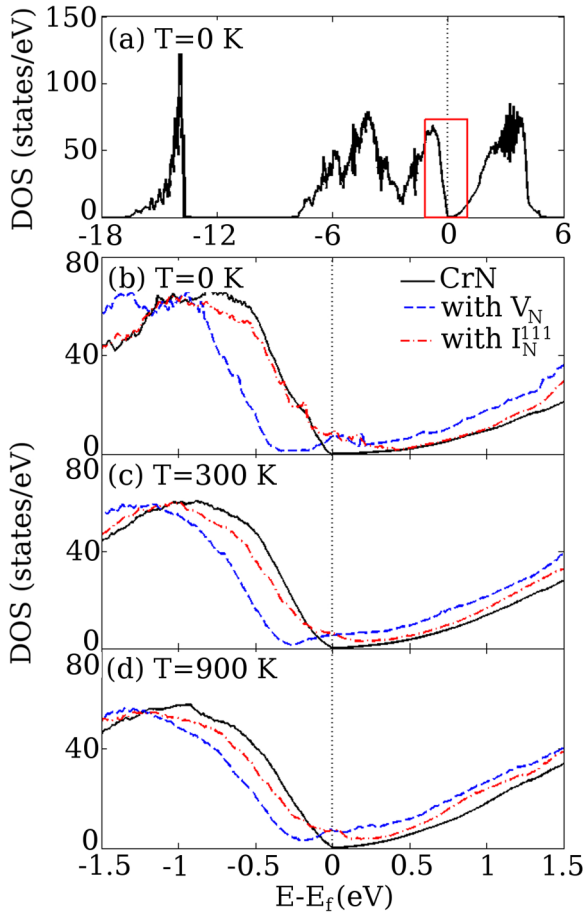

FIG. 6. (Color online) (a) Total density of states of CrN at $T = 0$ K obtained from static supercell DLM calculations. In order to have a detailed view of the region around the Fermi level, in (b)–(d) we show only the area that is marked with a red rectangle in (a). (b) DOS obtained in static calculations. We also show the total density of states of CrN obtained from DLM-MD calculations at temperatures (c) 300 K and (d) 900 K. The results are based on a 64-atom supercell with 32 Cr atoms and 31 (vacancy), 32 (defect-free), or 33 (interstitial) N atoms. The Fermi level, shown by the vertical dashed line, is aligned to zero.

line), nitrogen vacancy introduces a peak at around 0.2 eV. The peak primarily corresponds to Cr spin-down nonbonding states (above E_F) with a small admixture of N_p states. When a vacancy is present in the system, three electrons are released from the bonds between the neighboring Cr atoms and the nitrogen. They will increase the band filling which will lift the Fermi level towards the conduction band.

In the case of nitrogen interstitial, one can assume a CrN system with a vacancy in which the V_N is substituted with a nitrogen dimer instead. Assuming that the N-N dimer exhibits a double bond, as we discussed in the Results section, it leaves two electrons to bond with its Cr neighbors. The remaining one electron will increase the band filling as compared to defect-free CrN. Thus, adding a N interstitial will add one electron to the system. This is in agreement with the obtained results and can explain why the DOS in the case of N interstitial (red dash-dotted line in Fig. 6) is shifted just about to one-third of the shift one sees in the vacancy case (blue dashed line in Fig. 6) from its position in the ideal CrN (solid black line in Fig. 6) density of states. The apparent shift of the Fermi level towards the valence band, judged by the position of the DOS minimum, is just an artifact from the position of the defect state. Two peaks are visible around the Fermi energy at 0.02 and −0.07 eV. The peak at 0.02 eV corresponds to a combination of spin-up and spin-down Cr nonbonding states. The latter, −0.07 eV, pertains to the combination of Cr spin-up and -down nonbonding (below E_F) states. Both peaks exhibit some N_p character as well.

The aim of the paper is to study the effect of the defects on the electronic properties of paramagnetic cubic CrN at elevated temperatures. To obtain the density of states in this case, from DLM-MD calculations, we randomly extracted several MD samples. Then we calculated the density of state for each of them using a $5 \times 5 \times 5$ k grid and an energy cutoff of 500 eV. The total DOS is then derived by averaging over all these calculations.

Figures 6(c) and 6(d) show the total density of states from the DLM-MD calculations at two different temperatures, 300 and 900 K, respectively. At both temperatures, as can be seen, the gap has vanished due to the presence of defects. For the case of pure CrN DOS (black solid line in Fig. 6), it is difficult to draw a conclusion from our calculations at to what exact temperature the band gap closes. We can argue that the band gap of defect-free CrN is smeared out due to vibrations. However, at 900 K, the DOS at the Fermi level is clearly nonzero. At 300 K, our results indicate a border case where the band gap is about to close. The density of states around the Fermi level follows quite the same trend as in the static zero-temperature case [Fig. 6(b)], meaning that the nitrogen vacancy moves the Fermi level towards the conduction band. The same explanation applies for the N-interstitial case as discussed in the static case. The peaks which were present in the density of states at zero temperature, in the vacancy case, have vanished at higher temperatures, i.e., the temperature broadens the fine structure of the DOS at $T = 0$ K.

VI. CONCLUSION

We have applied a recently introduced model, DLM-MD, to study the formation energy, geometry, and electronic structure of the nitrogen defects in paramagnetic CrN as a function of temperature. We have calculated the formation energies of both nitrogen vacancy and interstitials. The vacancy formation energy does not show a strong dependence on temperature. However, the authors would like to underline that the role of the temperature in the N_2 gas-free energy is not considered in this set of calculations. The only stable N interstitial according to our calculations is the split bond in the ⟨111⟩ direction. The other two considered configurations transform to this position after, at most, a few picoseconds of simulation at finite temperature. Note that the formation energy for I_N^{111} increases as the temperature increases.

Detailed studies of the dynamics of N interstitials at elevated temperatures show that the I_N bonds to a nitrogen from the CrN matrix. The bond is stable and the N-N dimer oscillates around its center of mass, keeping its position. In other words, the N-N can rotate between different symmetry equivalent ⟨111⟩ directions.

In the case of N vacancy formation energy, there is a good agreement between the static calculations and DLM-MD. Thus, the static calculations can be trusted sufficiently enough to decide if the structure is stable. However, for N interstitials, the static calculations cannot be considered reliable enough to check the stability of the defect. As we have observed during our theoretical studies, for instance, the tetrahedral configuration can exist if we limit ourselves to the static approximation, while DLM-MD calculations reveal the instability for a defect in this position at room temperature and above.

Electronic structure calculations show that the ideal CrN exhibit a small band gap, indicating a semiconducting behavior in its cubic PM phase. The presence of N point defects closes this gap, resulting in density of states which show metallic characteristics. Both N vacancy and N interstitial act as donors, with V_N donating three electrons and I_N^{111} donating one electron to the system.

ACKNOWLEDGMENTS

We would like to assert our appreciation to Professor Lars Ojamäe for useful discussions. The authors would like to thank the Swedish National Infrastructure for Computing (SNIC) at the NSC center for providing the computational resources. The financial support from the Swedish Research Council (VR) through Grant No. 621-2011-4426 is gratefully acknowledged. B.A. acknowledges the financial support also from VR, Grant No. 621-2011-4417. I.A.A. is grateful for the Grant from the Ministry of Education and Science of the Russian Federation (Grant No. 14.Y26.31.0005) and Tomsk State University Academic D. I. Mendeleev Fund Program.

[1] J. Vetter, Surf. Coat. Technol. **76-77**, 719 (1995).
[2] A. Persson, J. Bergström, C. Burman, and S. Hogmark, Surf. Coat. Technol. **146-147**, 42 (2001).
[3] L. Corliss, N. Elliott, and J. Hastings, Phys. Rev. **117**, 929 (1960).
[4] F. Rivadulla, M. Bañobre López, C. X. Quintela, A. Piñeiro, V. Pardo, D. Baldomir, M. A. López-Quintela, J. Rivas, C. A. Ramos, H. Salva, J.-S. Zhou, and J. B. Goodenough, Nat. Mater. **8**, 947 (2009).
[5] S. Wang, X. Yu, J. Zhang, M. Chen, J. Zhu, L. Wang, D. He, Z. Lin, R. Zhang, K. Leinenweber, and Y. Zhao, Phys. Rev. B **86**, 064111 (2012).
[6] A. Filippetti, W. E. Pickett, and B. M. Klein, Phys. Rev. B **59**, 7043 (1999).
[7] A. Filippetti and N. A. Hill, Phys. Rev. Lett. **85**, 5166 (2000).
[8] D. Gall, C.-S. Shin, R. T. Haasch, I. Petrov, and J. E. Greene, J. Appl. Phys. **91**, 5882 (2002).
[9] R. Sanjinés, O. Banakh, C. Rojas, P. Schmid, and F. Lévy, Thin Solid Films **420-421**, 312 (2002).
[10] X. Y. Zhang and D. Gall, Phys. Rev. B **82**, 045116 (2010).
[11] P. A. Bhobe, A. Chainani, M. Taguchi, T. Takeuchi, R. Eguchi, M. Matsunami, K. Ishizaka, Y. Takata, M. Oura, Y. Senba, H. Ohashi, Y. Nishino, M. Yabashi, K. Tamasaku, T. Ishikawa, K. Takenaka, H. Takagi, and S. Shin, Phys. Rev. Lett. **104**, 236404 (2010).
[12] A. Herwadkar and W. R. L. Lambrecht, Phys. Rev. B **79**, 035125 (2009).
[13] B. Alling, T. Marten, and I. A. Abrikosov, Nat. Mater. **9**, 283 (2010).
[14] B. Alling, T. Marten, and I. A. Abrikosov, Phys. Rev. B **82**, 184430 (2010).
[15] P. Steneteg, B. Alling, and I. A. Abrikosov, Phys. Rev. B **85**, 144404 (2012).
[16] O. Hellman, P. Steneteg, I. A. Abrikosov, and S. I. Simak, Phys. Rev. B **87**, 104111 (2013).
[17] N. Shulumba, B. Alling, O. Hellman, E. Mozafari, P. Steneteg, M. Odén, and I. A. Abrikosov, Phys. Rev. B **89**, 174108 (2014).
[18] L. Zhou, F. Körmann, D. Holec, M. Bartosik, B. Grabowski, J. Neugebauer, and P. H. Mayrhofer, Phys. Rev. B **90**, 184102 (2014).
[19] A. Lindmaa, R. Lizárraga, E. Holmström, I. A. Abrikosov, and B. Alling, Phys. Rev. B **88**, 054414 (2013).
[20] B. Alling, Phys. Rev. B **82**, 054408 (2010).
[21] B. Alling, L. Hultberg, L. Hultman, and I. A. Abrikosov, Appl. Phys. Lett. **102**, 031910 (2013).
[22] L. Zhou, D. Holec, and P. H. Mayrhofer, J. Phys. D **46**, 365301 (2013).
[23] J. D. Browne, P. R. Liddell, R. Street, and T. Mills, Phys. Status Solidi (A) **1**, 715 (1970).
[24] P. Subramanya Herle, M. Hegde, N. Vasathacharya, S. Philip, M. Rama Rao, and T. Sripathi, J. Solid State Chem. **134**, 120 (1997).
[25] C. Constantin, M. B. Haider, D. Ingram, and A. R. Smith, Appl. Phys. Lett. **85**, 6371 (2004).
[26] J.-E. Sundgren, Thin Solid Films **128**, 21 (1985).
[27] J. H. Kang and K. J. Kim, J. Appl. Phys. **86**, 346 (1999).
[28] B. Subramanian, K. Prabakaran, and M. Jayachandran, Bull. Mater. Sci. **35**, 505 (2012).
[29] L. Hultman, Vacuum **57**, 1 (2000).
[30] P. Hones, N. Martin, M. Regula, and F. Levy, J. Phys. D **36**, 1023 (2003).
[31] G. Greczynski, J. Jensen, and L. Hultman, IEEE Trans. Plasma Sci. **38**, 3046 (2010).
[32] G. Kresse and J. Furthmuller, Phys. Rev. B **54**, 11169 (1996).
[33] G. Kresse and D. Joubert, Phys. Rev. B **59**, 1758 (1999).
[34] G. Kresse and J. Hafner, Phys. Rev. B **48**, 13115 (1993).
[35] J. Hubbard, Phys. Rev. B **19**, 2626 (1979).
[36] J. Hubbard, Phys. Rev. B **20**, 4584 (1979).
[37] J. Hubbard, Phys. Rev. B **23**, 5974 (1981).
[38] H. Hasegawa, J. Phys. Soc. Japan **46**, 1504 (1979).
[39] H. Hasegawa, J. Phys. Soc. Japan **49**, 178 (1980).
[40] B. L. Gyorffy, A. J. Pindor, J. Staunton, G. M. Stocks, and H. Winter, J. Phys. F **15**, 1337 (1985).
[41] V. I. Anisimov, J. Zaanen, and O. K. Andersen, Phys. Rev. B **44**, 943 (1991).

[42] S. L. Dudarev, G. A. Botton, S. Y. Savrasov, C. J. Humphreys, and A. P. Sutton, Phys. Rev. B **57**, 1505 (1998).
[43] S. Nosé, Prog. Theor. Phys. Suppl. **103**, 1 (1991).
[44] A. V. Ponomareva, Y. N. Gornostyrev, and I. A. Abrikosov, Phys. Rev. B **90**, 014439 (2014).
[45] S.-H. Jhi, S. G. Louie, M. L. Cohen, and J. Ihm, Phys. Rev. Lett. **86**, 3348 (2001).
[46] L. Tsetseris, N. Kalfagiannis, S. Logothetidis, and S. T. Pantelides, Phys. Rev. Lett. **99**, 125503 (2007).
[47] L. Tsetseris, N. Kalfagiannis, S. Logothetidis, and S. T. Pantelides, Phys. Rev. B **76**, 224107 (2007).
[48] See Supplemental Material at http://link.aps.org/supplemental/10.1103/PhysRevB.91.094101 for movies showing the dynamics of the N-N dimer in three different interstitial positions, at temperatures shown in Fig. 3. In the left side of the movie window, you can see the time evolution of the coordinates. In the right side, the N-N dimer fluctuations in the CrN lattice can be seen from different angles of view.